Journal of Applied Electrochemistry **30**: 845–853, 2000.
© 2000 *Kluwer Academic Publishers. Printed in the Netherlands.*

Zinc impregnation of the anodic oxidation layer of 1050 and 2024 aluminium alloys

J-P. DASQUET[1]*, J-P. BONINO[1], D. CAILLARD[2] and R.S. BES[1]
[1]*Laboratoire de Chimie des Matériaux Inorganiques et Energétiques, Université Paul Sabatier, UMR CNRS no. 5070 118, Route de Narbonne, 31062 Toulouse cedex, France*
[2]*Centre d'Elaboration des Matériaux et d'Etudes Structurales, UP CNRS 8011, 29 rue Jeanne Marvig, BP 4347, 31055 Toulouse cedex, France*
*(*author for correspondence, e-mail: jpdasquet@yahoo.fr)*

Received 20 May 1999; accepted in revised form 14 December 1999

Key words: alternating voltage, aluminium alloys, anodic oxidation, corrosion, impregnation, zinc

Abstract

The porous oxide layer obtained by phosphoric anodic oxidation (PAO) of 1050 and 2024T3 aluminium alloys is modified by impregnation with zinc under alternating voltage. The resulting current against applied voltage relationship shows that a threshold voltage is required to deposit the zinc. Beyond a low critical voltage, V_{c_L}, zinc electrocrystallization starts near the barrier layer and grows with time through the porous oxide layer whatever the alloy used as substrate. For the 2024T3 alloy, beyond a high critical voltage V_{c_H}, S.I.M.S. analysis shows that zinc is also present on top of the oxide layer. The distribution of zinc particles depends on the porous layer morphology: formation of zinc needles in a columnar form (1050 alloy) and dispersion of zinc particles in a disorganized structure (2024T3 alloy). The polarization curves obtained in a 3 wt % NaCl solution show a decrease in anodic and cathodic currents indicating a protective effect of zinc impregnation, confirmed by electrochemical impedance analysis.

1. Introduction

Anodic oxidation of aluminium alloys is extensively used in many applications to improve corrosion resistance. Several types of oxide layer can be obtained and can be roughly classified into two categories according to the reactivity of the coating formed on the electrolyte and, more exactly, according to the dissolving power of the electrolyte [1]. Thus, if the electrolyte is not aggressive, such as boric acid, the oxide layer formed is compact and uniform. In contrast, for sulphuric, chromic and phosphoric acid electrolytes, the coating obtained (depending on experimental conditions) consists of two parts. A compact uniform layer at the metal surface, the barrier layer, and a porous layer in contact with the electrolyte. Whatever the alloy, the oxide films are amorphous [2]. Although the thickness of each layer depends on the experimental conditions used, such as electrolyte composition and applied voltage, the morphology of the porous layer is very dependent on the composition of the aluminium alloy itself [3]. The corrosion properties of anodized aluminium alloys are frequently increased by hot sealing in chromic acid solution. Some authors [4, 5] have reported that the porous oxide layer with nanostructured porosity obtained on 1050 alloy can be modified by impregnation with metallic compounds under alternating voltage (50 Hz). Some authors have reported that physical properties, such as optical behaviour [6], can be modified by impregnating the porous oxide layer of anodised 1050 alloy with a metal, but the effects on the electrochemical properties have not been studied.

In this paper we describe zinc impregnation of phosphoric anodic oxidation (PAO) layers of 1050 and 2024T3 alloys (i.e., PAO_{1050} and PAO_{2024}). After microstructural characterization of the PAO layers, we compare the effects of zinc impregnation parameters on the composition, microstructure and reactivity in corrosive solution of PAO_{1050} and PAO_{2024}.

2. Experimental method

Before treatment, the aluminium alloys, 1050 (0.4 wt % Fe, 0.25% Si and 99.35% Al) and 2024T3 (4.4% Cu, 1.5% mg, 0.6% Mn and Al to 100%) were etched in alkaline solution at 60 °C followed by acid etching in a sulphuric acid/iron sulphate solution at 60 °C. Anodization was carried out in a phosphoric acid solution (0.8 M) at 15 V for 15 min at room temperature. Each of these operations was followed by washing in deionized water. Impregnation was carried out in a zinc sulphate based electrolyte ($ZnSO_4$:30 g L^{-1}, H_3BO_3:20 g L^{-1}, $MgSO_4$:20 g L^{-1}, $(NH_4)_2SO_4$:20 g L^{-1}), at room tem-

perature using alternating voltage (50 Hz) of varying amplitude between the working electrode and an inert auxiliary Ni electrode. The current distributions were recorded on an oscilloscope coupled to the alternating voltage generator. After processing, the sample was washed with deionized water and air dried.

Chemical analysis was performed on sample solutions by ionic chromatography and the distribution profiles of the elements were obtained by secondary ion mass spectrometry (Cameca IMS 6F/4F), by recording the spectra of the negative ions coupled with cesium, in order to cancel the signal deformation resulting from the oxidation state of the elements. The microstructure of the layers was observed in cross section by transmission electron microscopy (TEM) with a Jeol 2010 apparatus. The potentiodynamic analysis and electrochemical impedance spectroscopy studies were carried out in a thermostated corrosion cell containing 3 wt % NaCl solution.

3. Results and discussion

3.1. *Microstructural study of PAO_{1050} and PAO_{2024} layers*

The microstructures of PAO_{2024} and PAO_{1050} layers observed in cross section by TEM are reported in Figure 1. The dual microstructure of the PAO_{1050} layer, already reported by other authors [7], is made up of a compact thin layer (26 nm) close to the substrate, named the barrier layer, and a porous, thick layer, the thickness of which depends on the anodization time. The diameter of the pores was about 35 nm and the thickness of the cell wall about 30 nm. This columnar porosity, characteristic of PAO_{1050} layers, is very different to the disorganised porosity in PAO_{2024} layers, which probably results from the discontinuity of the barrier layer.

3.2. *Effect of impregnation parameters*

The electrochemical impregnation studied consists of depositing metal particles under alternating voltage in porous oxide layers obtained by PAO. Among the

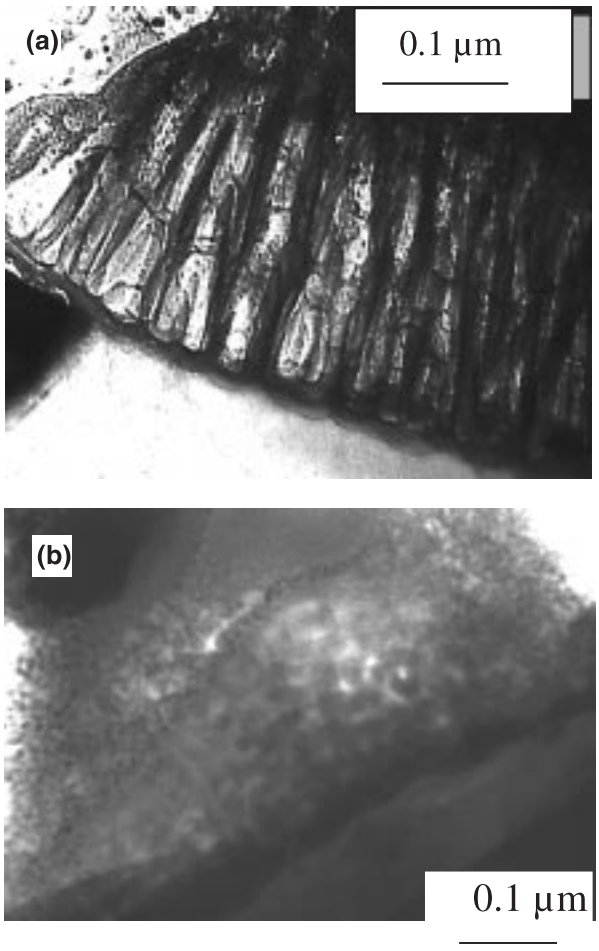

Fig. 1. Cross section of PAO_{1050} (a) and PAO_{2024} (b) by transmission electron microscopy.

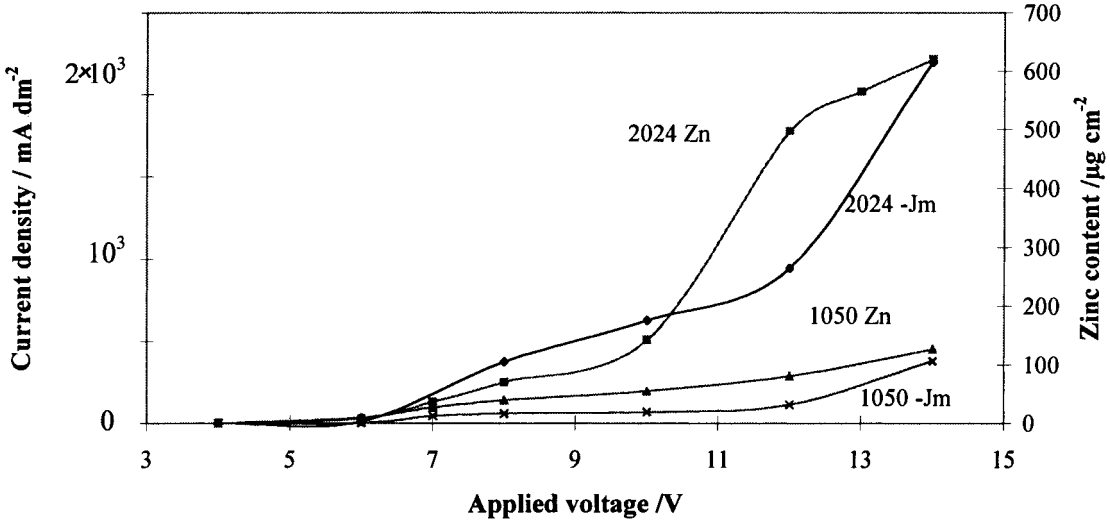

Fig. 2. Zinc content (Zn) and average current density (J_m) of impregnated PAO_{1050} and PAO_{2024} against applied alternating voltage.

processing parameters, we showed [8], for nickel impregnation of PAO layers on 1050, that voltage and impregnation time had a strong influence on metal inclusion in the porous layer. The higher compaction of the PAO_{2024} layer suggested it would be harder to deposit metal in it, so further investigations had to be made into the influence of voltage and impregnation time on the introduction of metal into the oxide layers.

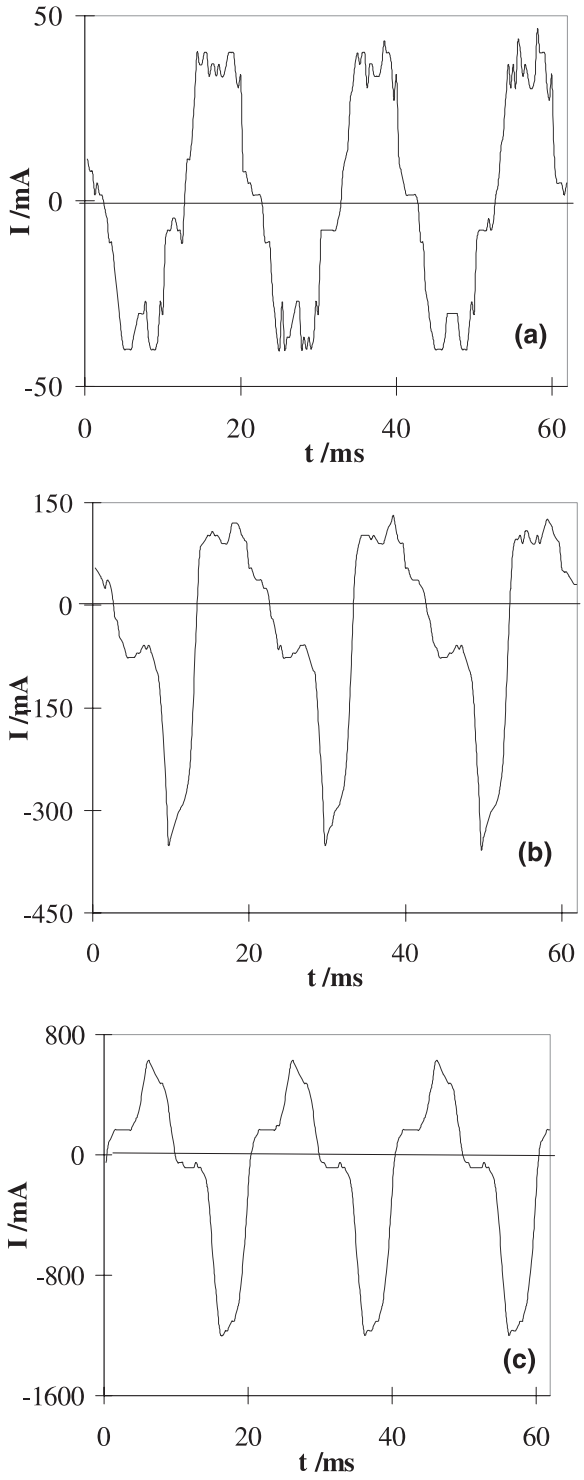

Fig. 3. Current oscillograms of PAO_{1050} layers for various alternating applied voltages: (a) 4, (b) 8 and (c) 12 V.

3.2.1. *Effect of applied voltage on current distribution and zinc deposition*

As shown in Figure 2, the quantity of zinc deposited increases with the intensity of the alternating voltage applied between the working and auxiliary electrodes. This result, obtained for an impregnation time of 5 min, shows a particular pattern for PAO_{2024} and reveals changes of slope at around 6 and 10 V. Up to 6 V, corresponding to low critical voltage (V_{c_L}), no resulting current appeared in the electrolytic cell and zinc was not deposited; beyond 6 V, the resulting current and the quantity of zinc deposited increased with the applied voltage. The increase of metal deposited is not a linear function of the applied voltage since a second critical voltage (V_{c_H}) appearing around 10 V, indicates the transition between two zinc deposition kinetics. In the same Figure, where resulting current densities (J_m) between the working and auxiliary electrodes are reported, the increase in zinc deposited at 10 V cannot be correlated to an increase in the resulting current. This imperfect correlation is not surprising if we consider that the current resulting from an alternating voltage is an average value between the anodic and cathodic parts, one of which does not result in reduction of zinc ions.

Figure 3 shows oscillograms of the current resulting from the application of 4, 8 and 12 V of 50 Hz alternating voltage for a PAO_{1050} layer (the evolution was the same for PAO_{2024} layers). From the oscillograms, we calculated the quantity of cathodic current which is plotted, in Figure 4, against the applied voltage. For both layers, the quantity of cathodic current closely follows the zinc content in the layer and the shape of the pulse allows the low and high critical voltages to be determined.

For both PAO_{1050} and PAO_{2024}, the distribution of the cathodic and the anodic parts of current pulse changes with applied voltage. These curves also provide characteristic slopes of the three voltage ranges previously defined from Figure 2. For both types of oxide layer, the anodic and cathodic parts of the current are comparable but present differences in amplitude.

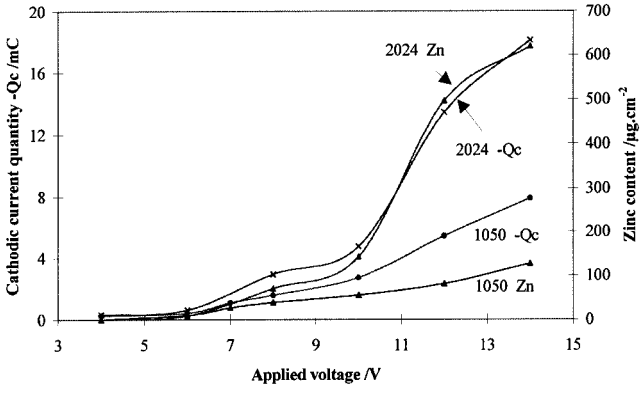

Fig. 4. Zinc content (Zn) and cathodic current quantity ($-Q_c$) against applied alternating voltage for PAO_{1050} and PAO_{2024} layers.

Below the low critical voltage V_{c_L}, for which the resulting average current is equal to zero, the anodic and cathodic parts of the curve are symmetric and the corresponding quantity of current probably contributes to the charge and discharge of the interface capacitance of the oxide layer. For these applied voltages, there is low or no charge transfer to reduce protons and zinc cations. Above this value, charge transfer and zinc deposition start to become effective. A distortion of the cathodic and anodic parts of the current appears. Its intensity depends on the PAO alloys. Above V_{c_L}, the cathodic distribution of the current is separated into two distinct parts. First, the cathodic current increases to a shoulder which can be associated to the charging of the capacitive porous oxide layer. After 4 or 5 ms a negative

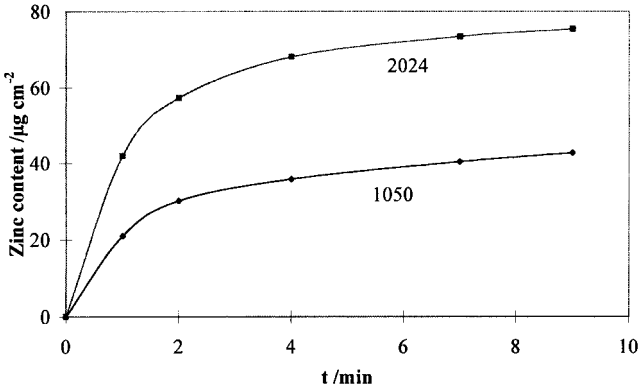

Fig. 6. Zinc content (Zn) against impregnation time for PAO_{1050} and PAO_{2024} ($V = 8$ V).

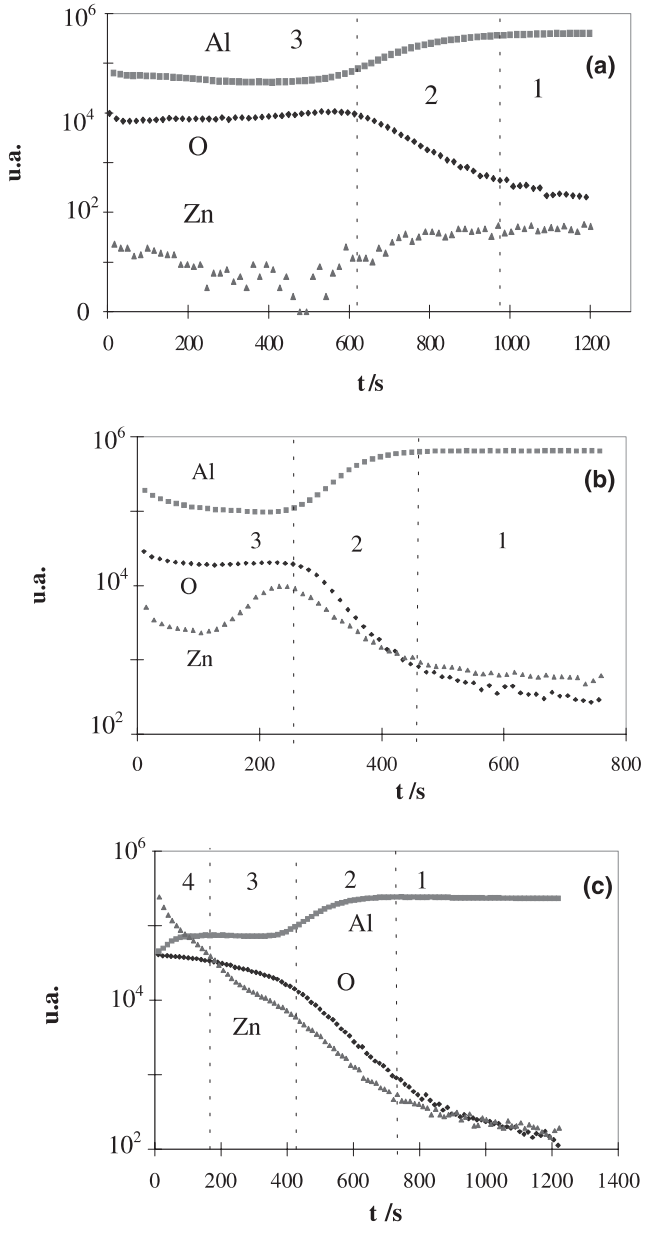

Fig. 5. S.I.M.S. analysis: concentration profiles of impregnated PAO_{2024} under various applied voltages: (a) 4, (b) 8 and (c) 12 V. Duration 3 min.

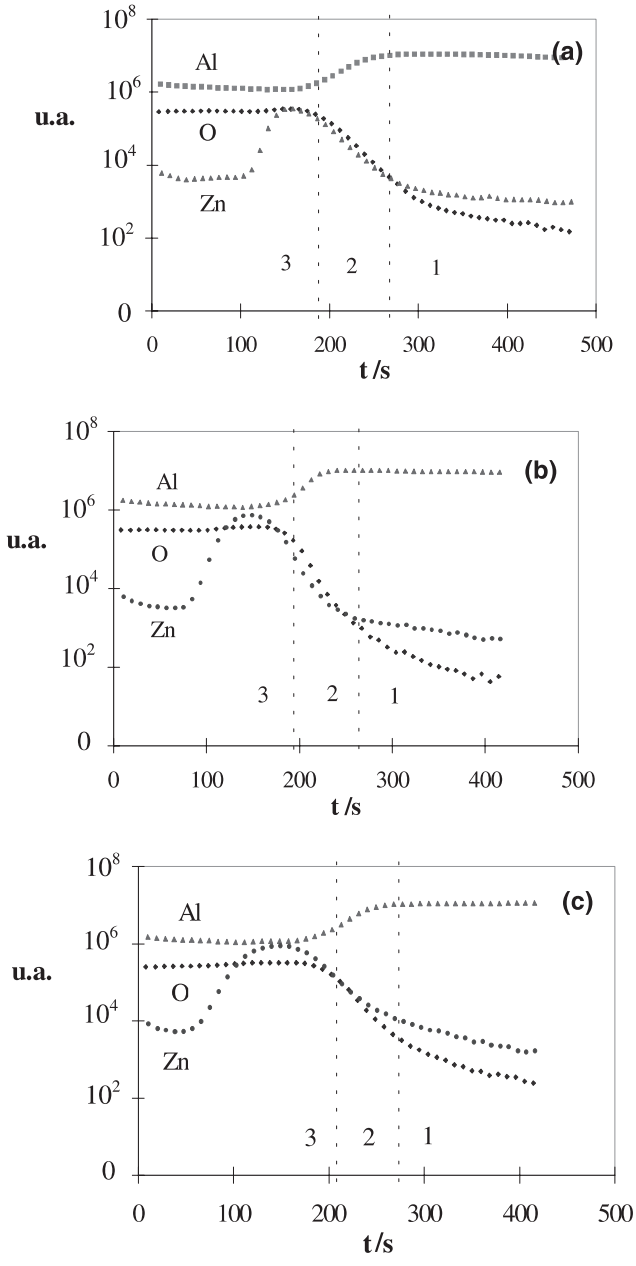

Fig. 7. S.I.M.S. analysis: concentration profiles for various impregnation times of PAO_{1050} under 8 V of applied alternating voltage. Impregnations: (a) 30 s, (b) 1 min and (c) 3 min.

peak of current occurs corresponding to charge transfer and deposition of zinc. When the applied voltage increases, we also notice a change in the anodic current distribution. This is particularly true for PAO_{1050}, in which, during the anodic pulse, after the capacitive discharge of the porous oxide layer, a current peak appears which is characteristic of the charge transfer required for the oxidation of zinc deposited during the cathodic pulse. For PAO_{2024}, the peak of anodic current is only obtained above the second critical voltage V_{c_H} (10 V). While the anodic and cathodic currents varied in the same way for PAO_{1050}, this was not the case for PAO_{2024} layers. When the applied voltage increased above V_{c_H}, the cathodic pulse was always separated into two distinct parts, but after capacitive charge of the porous oxide layer, the great increase in current characteristic of charge transfer was maintained during the whole cathodic pulse voltage. These changes of current distribution above V_{c_H} confirm the change in kinetics of cathodic and anodic reactions at the PAO_{2024} working electrode.

3.2.2. *Effect of applied voltage on zinc distribution in oxide layers*

To specify the distribution of zinc in the porous oxide layers, chemical analysis was carried out by SIMS. Figure 5 reports the profiles obtained for PAO_{2024} layers. With applied voltages lower than V_{c_L}, the absence of zinc from the oxide layer was confirmed for both alloys (Figure 5(a) shows the results for 2024T3 alloy), since the profiles of aluminium, oxygen and zinc are the same as those obtained on as-anodized substrate. The profiles are divided into three zones corresponding to (1) the aluminium substrate, (2) an interface zone where an increase in oxygen and a decrease in aluminium appear and (3) the oxide layer with stable quantities of aluminium and oxygen.

For applied voltages between V_{c_L} and V_{c_H} Figure 5(b), leading to a low zinc deposition rate, the profiles obtained show the presence of zinc at the interface zone. When the applied voltage rises to 11 V, the increase in zinc deposition in a zone close to the surface involves a significant accumulation of zinc on the external surface of the oxide layer. So, for impregnated PAO_{2024}, a fourth zone can be defined for which an increase of zinc and a decrease of aluminium occur, corresponding to zinc deposition on top of the zinc-modified oxide layer. This fourth zone did not appear for PAO_{1050} layers.

So, the study of the influence of the applied voltage showed, particularly for PAO_{2024}, two distinct voltage ranges for which the electrocrystallization of zinc takes

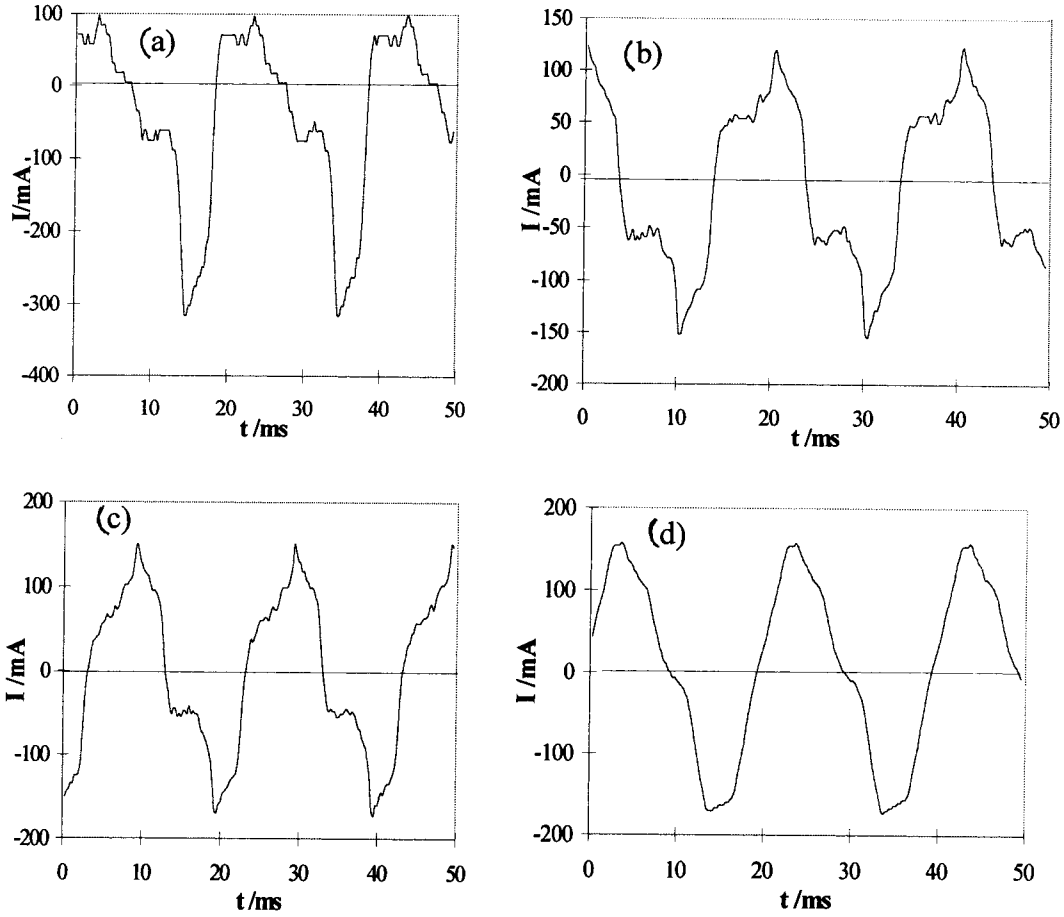

Fig. 8. Current oscillograms for various impregnation times of PAO_{1050} under 8 V applied alternating voltage. Impregnations: (a) 5 s, (b) 3 min, (c) 5 min and (d) 10 min.

place in a preferred region of the oxide layer. For voltages lower than V_{c_H}, zinc reduction takes place preferentially near the substrate-oxide interface, then for higher voltages, metal simultaneously appears on the outer oxide layer. We have attributed the strong rise in cathodic current when the applied voltage is increased above 11 V to a change in kinetics. This is now confirmed by a change in the region of the layer where zinc deposition takes place. For the more compact PAO_{2024} layer two distinct zones appeared beyond 12 V Figure 5(c), one corresponding to the impregnated oxide layer and the other to the zinc coating on top of it. To confirm zinc penetration into the oxide layer, for applied voltages between V_{c_L} and V_{c_H}, we followed the effect of impregnation duration.

3.2.3. *Effect of impregnation duration*

Figure 6 reports mass gain against impregnation time for PAO_{2024} and PAO_{1050} layers. An increase in deposited zinc appeared with impregnation time for both oxide layers.

Zinc penetration into porous PAO_{2024} and PAO_{1050} layers was followed by SIMS, against impregnation time under 8 V applied voltage (Figure 7 reports the profiles obtained for PAO_{1050} layers). For both alloys, the profiles showed that the region where deposition occured, initially at the substrate–oxide interface, shifted in time through the porous oxide layer towards the surface. For the PAO_{2024} layer, however, after 3 min of applied voltage, the profile of zinc in the layer showed that zinc deposition did not only occur near the substrate–oxide interface but also through the bulk of the oxide layer. It then rapidly reached the external region of the oxide layer without zinc deposition occuring on top of the layer.

Absence of bulk deposition in PAO_{1050} can be explained by the plot of current against duration of deposition (Figure 8). The distribution of cathodic and

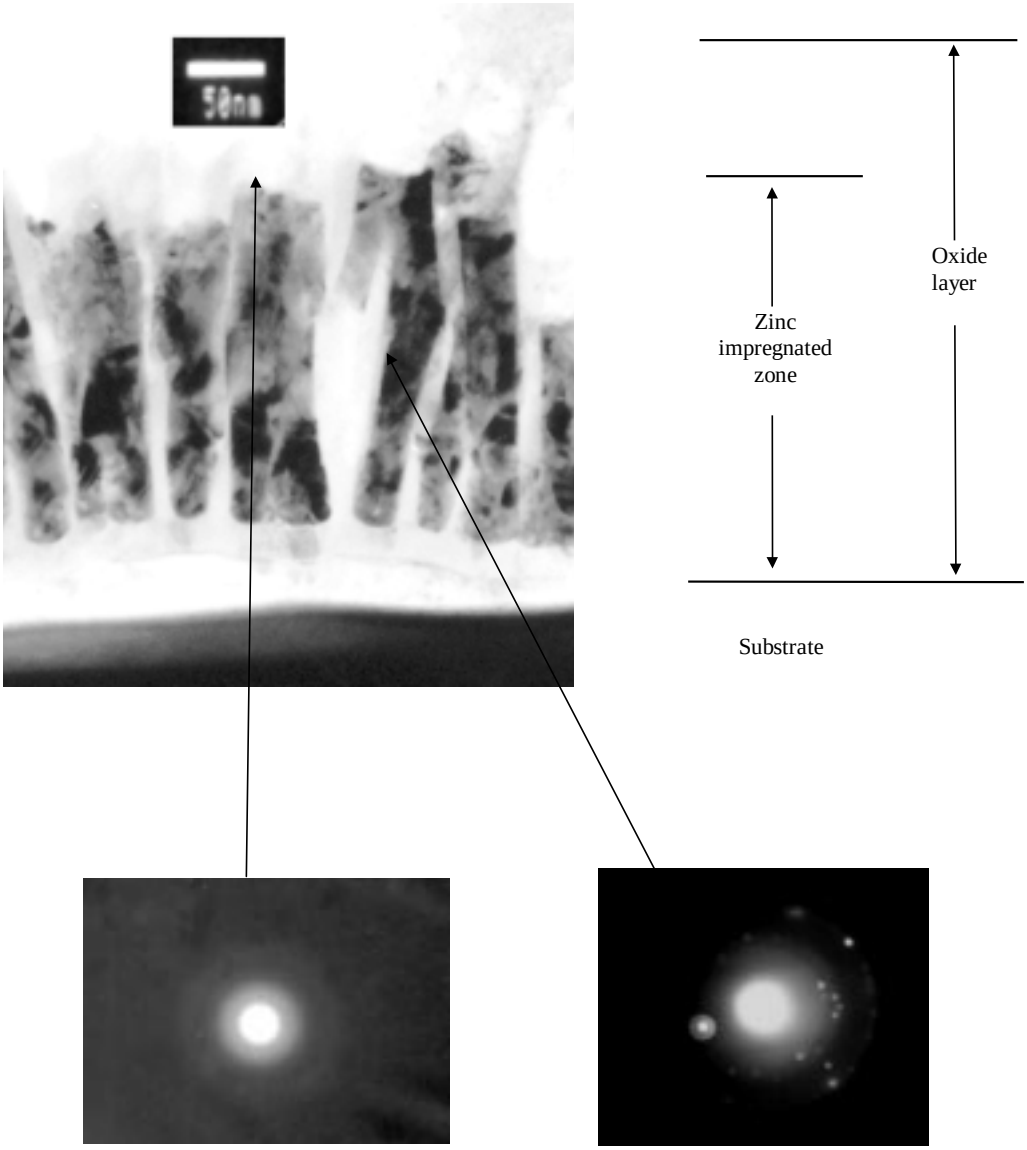

Fig. 9. Cross section of a zinc-impregnated PAO_{1050} layer ($V = 8$ V, $t = 5$ min) by transmission electron microscopy.

anodic current becomes symmetric after a deposition time for which the quantity of metal deposited in the oxide layer is sufficient to cancel its capacitive effect. In such conditions, part of the metal deposited during the cathodic pulse is etched during the following anodic pulse, explaining the saturation with time of metal deposition seen in Figure 6.

SIMS surface analysis showed that a similar metal distribution was obtained for both oxide layers. Although the presence of metal at the oxide-substrate interface has been frequently mentioned for PAO_{1050} layers, it has rarely been proved. We confirmed the SIMS results by transmission electron microscopy of both layers.

3.3. *Microstructural study*

Figures 9 and 10 report the micrographs showing the microstructures of PAO layers impregnated with zinc under 8 V alternating voltage for 5 min. For both types of porous layer, the dark particles observed in a zone close to the substrate-oxide interface have been identified as microcrystallized particles of zinc metal. The diffraction diagrams obtained in a zone far from the oxide–substrate interface (white part of the layers) indicate an amorphous structure as usually obtained by anodic oxidation of aluminium. We confirm here, that for both layers, zinc metal mainly appears in a region close to the oxide–substrate interface, more precisely just above the barrier layer.

The distribution of metal grains in oxide layers depends on the pore morphology. The growth of metallic zinc in PAO_{1050} is oriented by the anisotropy of the porosity and contributes to the formation of zinc needles of around 25 nm diameter, perpendicular to the surface. In the PAO_{2024} layer, the metal grains do not have such a well defined morphology but are homogeneously distributed through the interfacial region of the oxide layer.

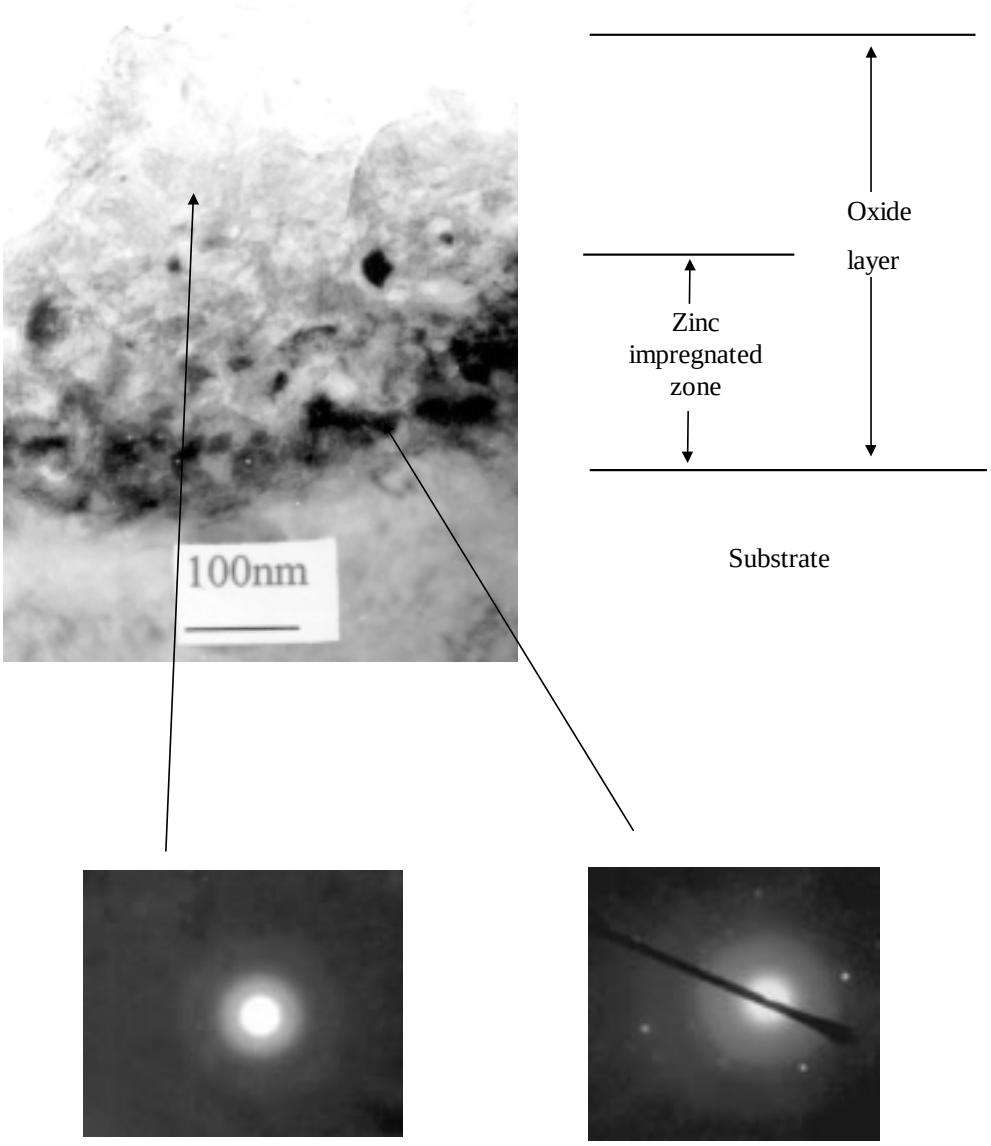

Fig. 10. Cross section of a zinc-impregnated PAO_{2024} layer ($V = 8$ V, $t = 5$ min) by transmission electron microscopy.

3.4. *Electrochemical study*

Figure 11 reports the polarization curves of PAO_{1050} and PAO_{2024} layers obtained in NaCl solution before and after zinc impregnation for 5 min under 8 V.

The protective effect of the phosphoric anodization of 2024 and 1050 alloys is clearly shown by the decrease in anodic and cathodic currents. The oxide layer covering the 2024 and 1050 alloys slows down the diffusion of protons and decreases the resulting cathodic current. The decrease of anodic current results from the attenuation of aluminium alloy oxidation through the oxide layer. Unexpectedly, zinc impregnation does not involve a shift in corrosion potential which would indicate sacrificial dissolution of zinc. The further decrease in cathodic and anodic currents reveals a protective effect of the zinc impregnation.

To pursue the study of impregnated PAO_{1050} and PAO_{2024} layers, we followed their behaviour by electrochemical impedance spectroscopy. From the Bode diagrams obtained (Figure 12), we determine a global resistance of the electrochemical interface [9] from the resistance values obtained at high and low frequencies (Table 1). The increase in global resistance of both layers confirms the protective effect of zinc impregnation. A forthcoming paper will report investigations by electrochemical impedance spectroscopy coupled to surface analysis to attempt to explain how zinc impregnation exerts its protective effect.

4. Conclusion

This study shows that zinc impregnation, under alternating voltage, of PAO layers can be carried out for both aluminium alloys 1050 and 2024T3. It also shows that the compactness of the oxide layer governs the location and the rate of zinc electrocrystallization.

The resulting current against applied voltage curves reveal two critical voltages, around 6 V (V_{c_L}) and 10V (V_{c_H}). V_{c_L} is the voltage for which a distortion of the cathodic part of the current appears corresponding to

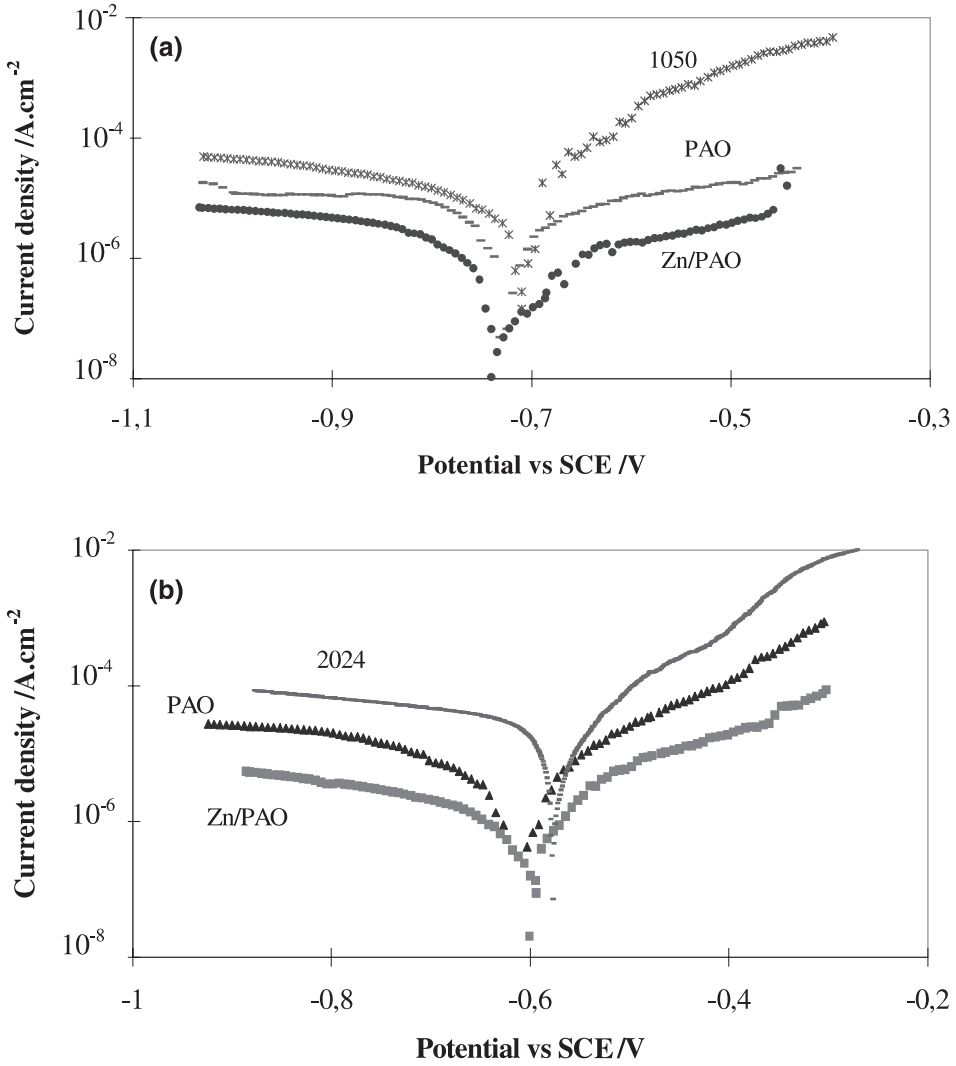

Fig. 11. Polarization curves obtained in a 3 wt % NaCl solution of anodized alloys and after zinc impregnation ($V = 8$ V, $t = 5$ min) of (a) PAO_{1050} and (b) PAO_{2024}.

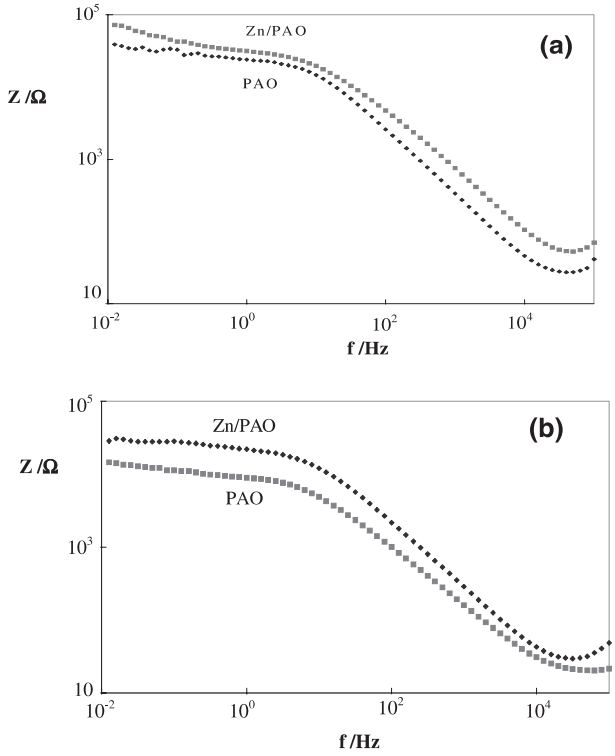

Fig. 12. Bode diagrams obtained in a 3 wt % NaCl solution of anodized alloys and after zinc impregnation ($V = 8$ V, $t = 5$ min) of (a) PAO_{1050} and (b) PAO_{2024}.

charge transfer through the porous oxide layer and to zinc deposition. Between V_{c_L} and V_{c_H}, electrodeposition takes place essentially near the substrate/oxide interface, whereas above V_{c_H} and particularly for the more compact PAO_{2024} layer, zinc deposition occurs on top of the oxide layer. This can be correlated to a change in current distribution. For an applied voltage of between V_{c_L} and V_{c_H}, for both layers, the deposition of zinc shifts with impregnation time from the substrate/oxide interface through the porous oxide layer towards its external part, but growth does not occur on top.

Table 1. Global resistance before and after zinc impregnation ($V = 8$ V, $t = 5$ min) for PAO_{1050} and PAO_{2024}

Global resistance/kΩ			
PAO_{1050}	Zn/PAO_{1050}	PAO_{2024}	Zn/PAO_{2024}
38.8	72.4	14.5	28.5

Transmission electronic microscopy shows the presence of particles in the oxide layer, essentially near the barrier layer, identified as microcrystallised zinc metal particles. Their distribution depends on the pore morphology: formation of needles in PAO_{1050} and more isotropic dispersed particles in PAO_{2024}.

An electrochemical study in NaCl solution showed the protective effect of zinc impregnation resulting from an increase in the global resistance of the electrochemical interface.

References

1. H. Keller, C. Hunter and D. Robinson, *J. Electrochem. Soc.* **100** (1953) 411.
2. M.C. Sainte Catherine, *in* T.S. Sudarshan and M. Jeandin (Eds), Proceedings STM8, Nice (1994), p. 1579.
3. J-P. Dasquet, 'Protection d'alliages d'aluminium contre la corrosion par imprégnation métallique de la couche d'oxydation ?tul> anodique', Thesis, Université P. Sabatier, Toulouse (1999).
4. C.R. Martin, *Science* **266** (1994) 1961.
5. T. Sato and S. Sakai, *Trans. Inst. Metal Finish.* **57** (1979) 43.
6. A. Andersson, O. Hunderi and C.G. Granqvist, *J. Appl. Phys.* **51**, 61 (1980) 754.
7. A. Baltat-Bazia, 'Etude de la texture des couches d'oxyde anodique sur l'aluminium en vue d'applications au collage', Thesis Paris VI (1992).
8. J. Salmi, 'Elaboration et caractérisation de couches absorbantes sélectives solaires sur l'alliage d'aluminium 1050', Thesis, Université P. Sabatier, Toulouse, (1999).
9. J. Hitzig, K. Jüttner and W.J. Lorenz, *J. Electrochem. Soc.* **133** (1986) 887.